AJNR

MR Imaging of the Extracranial Facial Nerve with the CISS Sequence

J.P. Guenette, N. Ben-Shlomo, J. Jayender, R.T. Seethamraju, V. Kimbrell, N.-A. Tran, R.Y. Huang, C.J. Kim, J.I. Kass, C.E. Corrales and T.C. Lee

MR Imaging of the Extracranial Facial Nerve with the CISS Sequence

J.P. Guenette, N. Ben-Shlomo, J. Jayender, R.T. Seethamraju, V. Kimbrell, N.-A. Tran, R.Y. Huang, C.J. Kim, J.I. Kass, C.E. Corrales, and T.C. Lee

ABSTRACT

BACKGROUND AND PURPOSE: MR imaging is not routinely used to image the extracranial facial nerve. The purpose of this study was to determine the extent to which this nerve can be visualized with a CISS sequence and to determine the feasibility of using that sequence for locating the nerve relative to tumor.

MATERIALS AND METHODS: Thirty-two facial nerves in 16 healthy subjects and 4 facial nerves in 4 subjects with parotid gland tumors were imaged with an axial CISS sequence protocol that included 0.8-mm isotropic voxels on a 3T MR imaging system with a 64-channel head/neck coil. Four observers independently segmented the 32 healthy subject nerves. Segmentations were compared by calculating average Hausdorff distance values and Dice similarity coefficients.

RESULTS: The primary bifurcation of the extracranial facial nerve into the superior temporofacial and inferior cervicofacial trunks was visible on all 128 segmentations. The mean of the average Hausdorff distances was 1.2 mm (range, 0.3–4.6 mm). Dice coefficients ranged from 0.40 to 0.82. The relative position of the facial nerve to the tumor could be inferred in all 4 tumor cases.

CONCLUSIONS: The facial nerve can be seen on CISS images from the stylomastoid foramen to the temporofacial and cervicofacial trunks, proximal to the parotid plexus. Use of a CISS protocol is feasible in the clinical setting to determine the location of the facial nerve relative to tumor.

The facial nerve, which exits the skull base at the stylomastoid foramen and then branches within the parotid gland, is the primary motor nerve for facial expression. According to a recent systematic review, >20% of patients undergoing primary parotidectomy experience immediate postoperative facial weakness, while almost 4% experience permanent facial weakness, even with the use of intraoperative facial nerve monitoring.[1] With an incidence of parotid gland tumors of 4.8 per 100,000 individuals per year[2] or an incidence of approximately 15,500 per year in the United States, it can be inferred that thousands of patients may experience facial nerve injury during parotid operations each year in the United States alone. Iatrogenic facial nerve injury also regularly occurs during oral, maxillofacial, and cosmetic surgery.[3] Moreover, due to concern for facial nerve injury, it is generally considered unsafe to perform image-guided core biopsy of deep head and neck lesions if traversal of the retromandibular/parotid space is required.[4] Image-guided cryoablation of head and neck tumors, a relatively new treatment approach,[5] is similarly limited. On the opposite end of the treatment spectrum, face transplant requires facial nerve anastomosis[6] or facial nerve transfer[7] to enable motor function of the transplanted structures.

MR imaging can be used to visualize the intracranial cisternal and canalicular portions of the facial nerve[8] as well as the segments of the facial nerve in the temporal bone.[9] However, the intraparotid facial nerve distal trunk and branches are not consistently visible on conventional MR or CT images,[10-12] even when the MR imaging signal and resolution are maximized using a localized surface coil.[13] Currently, no MR imaging method is routinely used to image the facial nerve. However, the CISS sequence has previously been demonstrated to enable visualization of the

○━ Indicates open access to non-subscribers at www.ajnr.org

▤ Indicates article with supplemental on-line table.

◨ Indicates article with supplemental on-line photos.

http://dx.doi.org/10.3174/ajnr.A6261

intracranial portions of the facial nerve[14] as well as the recurrent laryngeal and vagus nerves in the neck.[15] Anecdotal evidence has also shown that the extraforaminal segments of the cranial nerves can be visualized with the CISS sequence.[16] We therefore hypothesized that the CISS sequence may have a role in routine preoperative evaluation of the extracranial facial nerve.

The aims of this study were 2-fold: 1) to determine the extent of the extracranial facial nerve that can be confidently and routinely visualized with a CISS sequence protocol; and 2) to identify the potential clinical utility of incorporating the CISS protocol in routine parotid tumor imaging for preoperative evaluation of nerve location.

MATERIALS AND METHODS

Twenty healthy subjects were enrolled in this prospective study, which was designed to determine the extent of the extracranial facial nerve that can be confidently and routinely visualized with a CISS sequence protocol. All healthy individuals were eligible for participation with the following exclusion criteria: younger than 18 years of age, pregnant, history of head and neck cancer, history of parotid gland pathology including parotitis, and inability to have an MR imaging examination. All healthy subjects underwent a 1-hour 3T MR imaging examination of the face between December 2017 and June 2018. All subjects provided informed consent. This prospective study was approved by our institutional review board and was performed in compliance with Health Insurance Portability and Accountability Act.

In addition, to identify the potential clinical utility of incorporating the CISS protocol in routine parotid tumor imaging, a retrospective review was performed of images obtained on consecutive patients with parotid tumors in the clinical setting between August 2018 and October 2018, when the CISS sequence was included as part of a proposed new parotid tumor MR imaging protocol. This retrospective study was separately approved by our institutional review board and was also performed in compliance with the Health Insurance Portability and Accountability Act with waiver of informed consent.

Imaging Protocol

All MR imaging examinations were performed on a Magnetom Prisma 3T MR imaging system with a 64-channel head/neck coil (Siemens, Erlangen, Germany). An axial CISS sequence was performed without intravenous contrast from the stylomastoid foramen to the lower aspect of the parotid gland, which, for practicality and repeatability, can be approximated from the mid-basiocciput to the cranial aspect of the extrinsic tongue muscles (Fig 1). Multiple slightly variant CISS protocols were performed on the first 10 healthy subjects. A single protocol was subjectively identified as the most promising; therefore, that protocol was included in all subsequent subject examinations. The protocol parameters are included in the Table. Of note, when the CISS protocol was added to the clinical parotid MR imaging protocol, the FOV was inadvertently decreased to 180 mm, resulting in higher spatial resolution but a lower signal-to-noise ratio compared with the images acquired with a 240-mm FOV in the healthy subjects.
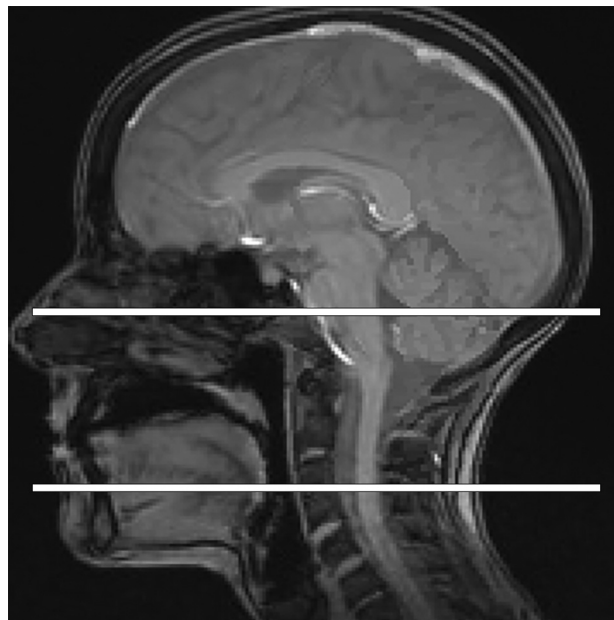
FIG 1. Sagittal midline localizer MR image. *Horizontal white lines through the basisphenoid and cranial aspect of the extrinsic tongue muscles serve as an accurate approximation for the CISS craniocaudal slab selection when imaging the facial nerve.*

Parameters for CISS sequence

Parameter	
TR	4.97 ms
TE	2.19 ms
Averages	1
Section thickness	0.8 mm
FOV	240 × 240
Matrix	320 × 320
Voxel size	0.8 × 0.8 × 0.8 mm
Bandwidth	521 Hz/pixel
Flip angle	33°
Elliptic scanning	On
Acquisition time	4:44 minutes

Facial Nerve Segmentation

Four observers independently segmented the facial nerve from the stylomastoid foramen (Fig 2) to the most distal aspect of the intraparotid branches that they could confidently identify. The observers were a neuroradiologist with 7 years of postfellowship dedicated clinical neuroradiology experience (observer 1), a neuroradiologist with 3 years of postfellowship dedicated clinical neuroradiology experience (observer 2), a first-year radiology resident (observer 3), and a fourth-year medical student (observer 4). All nerve segmentations were performed in the open-source image-processing software 3D Slicer (Version 4.8.1; www.slicer.org). The segmentations were performed in the 3D Slicer editor module. This module allows simultaneous visualization of the axial 0.8-mm images, coronal 0.8-mm reformatted images, and sagittal 0.8-mm reformatted images. The observers were allowed to build the segmentation using all 3 planes. Image manipulation or postprocessing, such as the creation of minimum intensity projection images, was
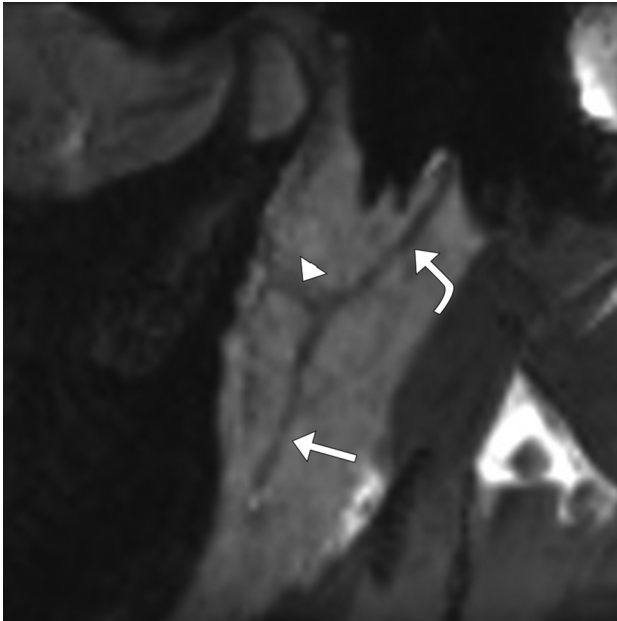
FIG 2. Representative sagittal-oblique CISS minimum intensity projection MR image shows the visible course of the facial nerve trunk (*curved arrow*) from the stylomastoid foramen to the distal aspects of the temporofacial (*arrowhead*) and cervicofacial (*arrow*) trunks.

not allowed, to best simulate the practical clinical environment in which such tools may not be available.

Facial Nerve Segmentation Comparisons

All segmentations were reviewed to determine the number of branches identified. To determine similarity of the tracings, we compared segmentations by calculating average Hausdorff distance values[17] and Dice coefficients.[18] Average Hausdorff distance values provide a measurement of the average distance of the points in one segmentation to the corresponding closest points in another segmentation. Dice coefficients provide a measurement of the degree of overlap of the segmentation volumes. In addition, the length of each segmentation from the stylomastoid foramen to the most distal aspect of the cervicofacial trunk was measured and compared. The segmentations of the more senior neuroradiologist (observer 1) were used as the reference for all comparisons.

Retrospective Review of Clinical Examinations

The CISS images were reviewed and facial nerves were followed by a single observer to evaluate whether the position of the facial nerve could be identified relative to the known tumor. The observed purported relative location of the nerve was communicated to the surgeon before the operation. Following the operation, the surgeon confirmed the actual location of the nerve relative to the tumor.

RESULTS

Twenty healthy subjects (15 men, 5 women; 30.4 ± 7.7 years of age; age range, 20–50 years) were enrolled. The optimized CISS protocol, as described in the Materials and Methods section, was performed on 16 of the healthy subjects (12 men, 4 women;

31.4 ± 8.5 years of age; age range, 20–50 years). Due to imaging time constraints, protocol optimization, and the testing of several other sequences, this sequence was not performed in 4 subjects. A total of 32 facial nerves, 2 per healthy subject, were thus imaged.

The CISS images were retrospectively reviewed for 4 consecutive patients who underwent clinical MR imaging examinations with a parotid protocol for a known parotid mass. These patients were the following: a 55-year-old man with a recurrent right parotid Warthin tumor, an 83-year-old woman with a left parotid poorly differentiated carcinoma with sarcomatoid features, a 32-year-old woman with a left parotid pleomorphic adenoma, and a 75-year-old woman with a right parotid Warthin tumor.

All images are available for review and further analysis through the Harvard Dataverse.[19]

Facial Nerve Segmentation Comparisons

The primary bifurcation of the facial nerve into the superior temporofacial and inferior cervicofacial trunks was visible on all 128 segmentations (32 nerves each segmented by 4 observers) along with at least the proximal aspect of these 2 trunks (Fig 3). The classically taught more distal 5 branches were not visualized on the segmentations.

The mean of the average Hausdorff distances was 1.2 mm (range, 0.3–4.6 mm) overall, 0.9 mm (range, 0.3–3.3 mm) when comparing observers 1 and 2, 1.7 mm (range, 0.3–4.6 mm) when comparing observers 1 and 3, and 1.0 mm (range, 0.3–2.1 mm) when comparing observers 1 and 4. Dice coefficients ranged from 0.40 to 0.82 with means of 0.64, 0.57, and 0.59 when comparing observer 1 with observers 2, 3, and 4, respectively. Segmentation lengths varied on average by 5.8 ± 4.8 mm overall, 5.7 ± 4.9 mm (18% ± 17%) when comparing observers 1 and 2, 5.1 ± 4.6 mm (16% ± 14%) when comparing observers 1 and 3, and 6.6 ± 4.9 mm (21% ± 15%) when comparing observers 1 and 4. All Hausdorff distances, dice coefficients, length difference percentages, and segmentation volume difference percentages are reported in the On-line Table. Graphic demonstration of the interobserver data distributions is presented in On-line Figs 1–4.

All measurement data are available for review and further analysis through the Harvard Dataverse.[19]

Retrospective Review of Clinical Examinations

The main facial nerve trunk and/or the temporofacial or cervicofacial trunk could be followed from the stylomastoid foramen to the level of the tumor in all cases, and the relative position of the facial nerve to the tumor could be inferred in all cases (Fig 4). The facial nerve location relative to the tumor was confirmed by the operating surgeon for the 3 patients who underwent tumor resection. One patient has elected observation of a Warthin tumor; therefore, surgical confirmation of nerve location has not been obtained.

DISCUSSION

In this study, 4 observers of variable expertise were each able to trace the facial nerve on the CISS images from the stylomastoid foramen through the primary bifurcation and along at least the
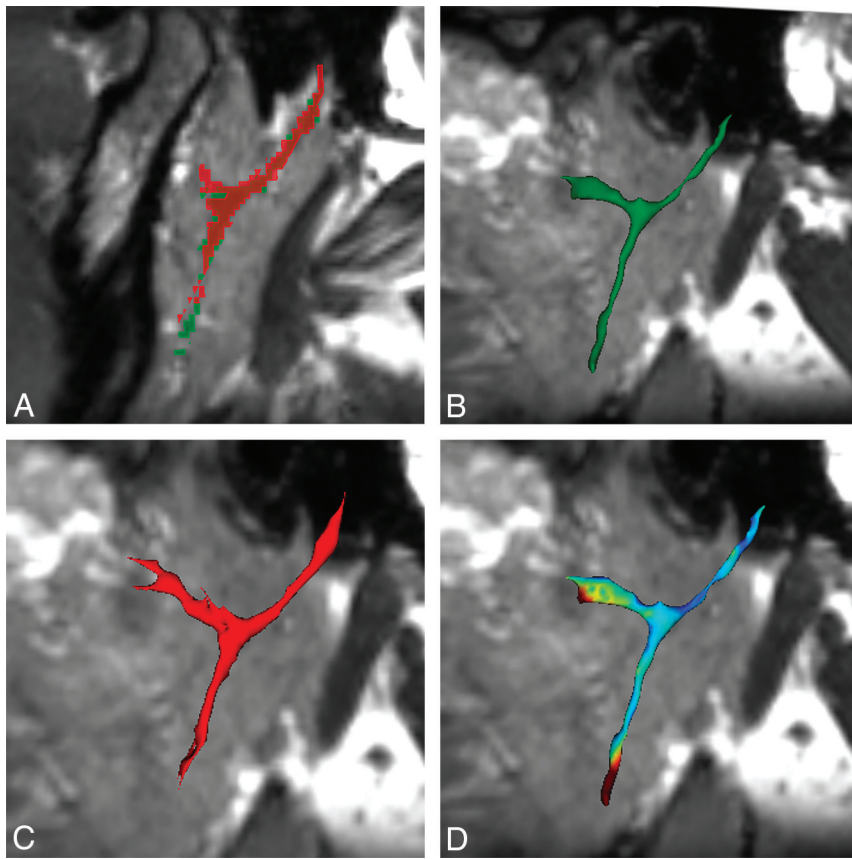
FIG 3. Representative segmentations of the left facial nerve of subject 20 with an average Hausdorff distance of 0.64, Dice coefficient of 0.60, length difference of <1%, and segmentation volume difference of 8%. *A*, Segmentations of observer 1 (*green outline*) and observer 4 (*red outline*) superimposed on the CISS image show similar agreement along the main nerve root, bifurcation, and proximal aspects of the temporofacial and cervicofacial roots, with more distal variability along the cervicofacial root, even despite the similar length segmented. *B*, 3D rendering of the observer 1 segmentation. *C*, 3D rendering of the observer 4 segmentation. *D*, Dice overlap map shows the spectrum of agreement, with blue being good agreement and red being poor agreement.

Comparison with Current Literature on Facial Nerve Imaging

This study advances prior published work that has also aimed to identify and evaluate the extracranial facial nerve. It has been known since the early and mid-1990s that the proximal extracranial facial nerve trunk can be routinely visualized and that gadolinium-based contrast is not helpful.[10,11] Steady-state imaging with the gradient-recalled acquisition in steady state sequence[12] and double-echo steady-state with water excitation sequence[20] have previously been reported for facial nerve imaging with more inconsistent identification of the cervicofacial and particularly temporofacial trunks, though the double-echo steady-state with water excitation sequence has recently been shown to allow accurate categorization of tumor location to the superficial or deep parotid lobes.[21] Our success in this study may be attributable to the use of more technologically advanced hardware. Use of a PSIF-DWI sequence to visualize at least a portion of the cervicofacial and temporofacial branches has more recently been described,[13] and the images obtained with the CISS protocol (eg, Fig 2) seem comparable with the published PSIF-DWI, which was obtained with a small surface coil and postprocessed into MPR and MIP images. As part of this study, we attempted PSIF-DWI but could not replicate the prior results. Moreover, our goal was to enable facial nerve imaging as part of a routine MR imaging examination, and we considered the use of a localized surface coil or manual postprocessing to be insufficient.

Anecdotally, we were able to visualize the facial nerve with 3D T1 sampling perfection with applications-optimized contrasts by using different flip angle evolutions (SPACE sequence; Siemens) images, but further protocol optimization and more rigorous testing would be needed for comparison with the CISS protocol. We could not discern any contrast between the facial nerve and surrounding parotid gland tissue with the pointwise encoding time reduction with radial acquisition (PETRA) sequence, which has been used to visualize the nerve through the temporal bone.[9]

Inherent Facial Nerve Anatomy Imaging Limitations

Confident identification of the more distal branches of the facial nerve seems to be hindered primarily by 3 factors: 1) the small size of the nerve fibers in the intervening parotid plexus that are below the resolution of current practical clinical imaging; 2)
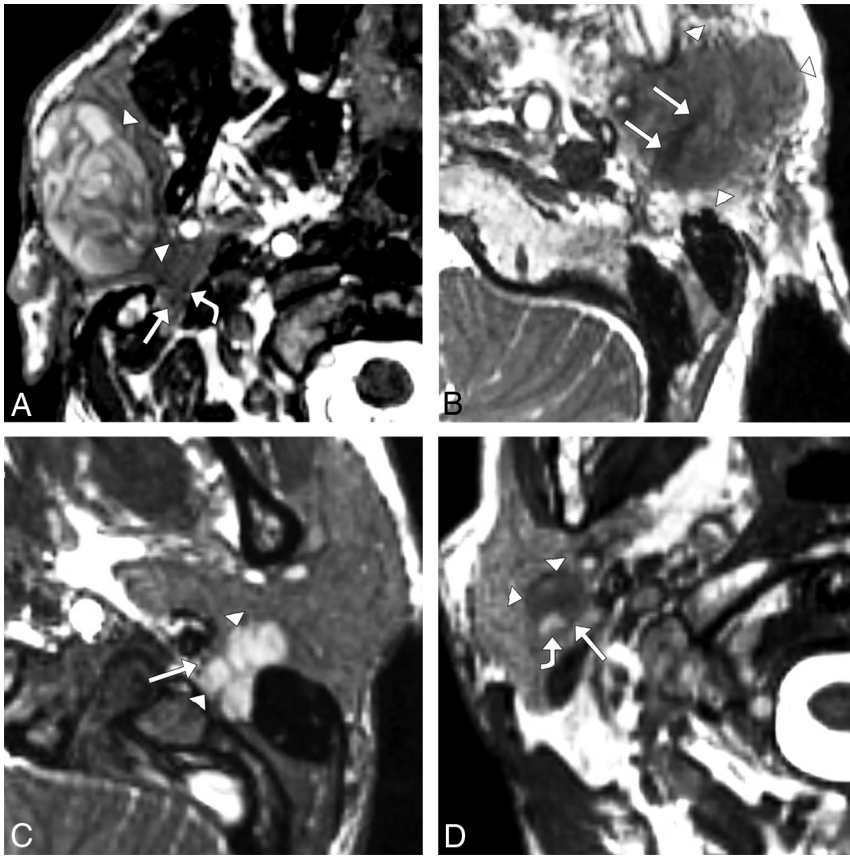
proximal temporofacial and cervicofacial trunks in all 32 facial nerves of the healthy subjects. The average Hausdorff distance of 1.2 mm is very close to the 0.8-mm isotropic voxel dimensions of the CISS images, indicating that the observers' nerve tracings varied, on average, by only 1.5 voxels. The Dice coefficients, which are a measure of segmentation overlap, are reasonable, given that segmentations in 3D Slicer are voxel-based and the facial nerve frequently crosses through portions of several voxels on a single section leading to inherent section-by-section segmentation variability. In addition, the location of the facial nerve primary or secondary trunks could be inferred relative to the tumor in the 4 patients scanned with the CISS protocol, and this location was confirmed in the 3 patients who underwent an operation. Although the more distal facial nerve branches were not visualized, surgeons typically identify the facial nerve proximal to the tumor, create a dissection plane along the nerve trunks, and may never identify the smaller parotid plexus rootlets or distal branches, so the portions of nerve visualized in this study should be adequate for surgical planning in most cases.

FIG 4. Axial CISS images in patients with parotid gland tumors. *A*, A 55-year-old man with a right parotid gland, 35 × 22 × 44 mm (anteroposterior × transverse × craniocaudal) Warthin tumor (*arrowheads*) and temporofacial (*straight arrow*) and superiorly displaced cervicofacial (*curved arrow*) trunks of the facial nerve (*straight arrow*), apparently deep to the tumor and just posterior to the retromandibular vein. In the operating room, the distal branches of the facial nerve were confirmed to be in the plane of the tumor with distal divisions displaced above and below the tumor and with superior displacement of the parotid plexus. *B*, An 83-year-old woman with left parotid gland, 23 × 21 × 29 mm poorly differentiated carcinoma with sarcomatoid features (*arrowheads*) and an apparently expanded facial nerve with irregular margins (*arrows*) coursing through the tumor, suggestive of perineural tumor invasion. A radical parotidectomy was performed, and pathology analysis confirmed extensive perineural invasion. *C*, A 32-year-old woman with a left parotid gland 18 × 19 × 24 mm pleomorphic adenoma (*arrowheads*) extending into the stylomastoid foramen and anteromedially displacing the facial nerve (*arrow*). Due to these imaging findings, a postauricular infratemporal fossa surgical approach was used, confirming the location of the nerve and confirming impingement of the nerve as it entered the stylomastoid foramen. *D*, A 75-year-old man with a right parotid gland, 12 × 11 × 19 mm Warthin tumor (*arrowheads*) just superficial to and between the distal, small-caliber, low-signal cervicofacial trunk of the facial nerve (*straight arrow*) and high-signal retromandibular vein (*curved arrow*). This patient has elected observation, and there is thus no surgical confirmation of facial nerve location.

into many small rootlets, which form a parotid plexus.[22] These parotid plexus rootlets ultimately join into the 5 classically taught branches: temporal, zygomatic, buccal, marginal mandibular, and cervical. However, these branches are variable and are often present in duplicate or triplicate.[22]

Study Limitations

The major primary limitation of this study is the absence of a criterion standard comparison. The scientifically ideal study would corroborate intraoperative nerve mapping with preoperative and intraoperative MR imaging nerve delineation, but the ethical approval of such a study would depend on the involved added surgical/anesthesia time and risk. As with other similar studies, we contend that this study is an adequate surrogate, given the known course of the facial nerve and the easily identifiable expected location of the proximal extracranial nerve at the stylomastoid foramen. Another limitation of the technical portion of this study is that all imaging examinations were performed on a single MR imaging system that is currently one of the highest caliber systems on the market with high gradients; therefore, the results may not be replicable on older systems or systems from other vendors with similar, but not identical, sequences. In addition, the CISS protocol used in our clinical examination was inadvertently performed with a 180-mm FOV, instead of the 240-mm FOV used in the healthy subjects. Returning to the higher signal-to-noise 240-mm FOV may or may not improve visualization of the facial nerve in patients.

In this study, only 4 patients with parotid tumors were imaged with the CISS facial nerve sequence, and only 3 of these patients underwent an operation with subsequent surgical confirmation of facial nerve location. Consequently, although delineation of the facial nerve was possible in each of these patients, the generalizability in a routine patient population remains unknown. There may also be inherent limitations with the CISS sequence. Although discrimination of the low-signal facial nerve from large, generally high-signal blood vessels is relatively straightforward, some larger veins and many smaller blood vessels also have low signal. The signal of the parotid duct system is also variable, with high

variant terminal branch anatomy, including variation in the number and location of the branches, which precludes identification based on location; and 3) difficulty discriminating small nerve fibers, small ducts, and small vessels. A comprehensive overview of the parotid plexus, also known as the pes anserinus, and variant facial nerve anatomy has been recently published on the basis of a study of 158 human cadaver dissections.[22] On the basis of this work and prior work, it is known that the facial nerve exits the skull base at the stylomastoid foramen and then divides into a superior temporofacial trunk and an inferior cervicofacial trunk, usually within the parotid gland. These trunks then divide

signal in some subjects and low signal in others. High signal in the ducts could perhaps be obtained routinely by preparing a subject with a lemon mouth swab, as previously reported for MR sialography.[23] The small fibrous septations between gland lobules are at the limits of resolution of the CISS images as performed and, therefore, are also difficult to distinguish from nerve as the nerve roots decrease in size and branch into the plexus.

CONCLUSIONS

The results of this study suggest that the facial nerve can be routinely followed from the stylomastoid foramen to the temporofacial and cervicofacial trunks, proximal to the parotid plexus, with a CISS imaging protocol. Moreover, use of a CISS protocol is feasible in the clinical setting to determine the location of the primary and secondary trunks of the facial nerve relative to a tumor.

REFERENCES

1. Sood AJ, Houlton JJ, Nguyen SA, et al. **Facial nerve monitoring during parotidectomy: a systematic review and meta-analysis.** *Otolaryngol Head Neck Surg* 2015;152:631–67 CrossRef Medline
2. Pinkston JA, Cole P. **Incidence rates of salivary gland tumors: results from a population-based study.** *Otolaryngol Head Neck Surg* 1999;120:834–40 CrossRef Medline
3. Hohman MH, Bhama PK, Hadlock TA. **Epidemiology of iatrogenic facial nerve injury: A decade of experience.** *Laryngoscope* 2014; 124:260–65 CrossRef Medline
4. Gupta S, Henningsen JA, Wallace MJ, et al. **Percutaneous biopsy of head and neck lesions with CT guidance: various approaches and relevant anatomic and technical considerations.** *Radiographics* 2007;27:371–90 CrossRef Medline
5. Guenette JP, Tuncali K, Himes N, et al. **Percutaneous image-guided cryoablation of head and neck tumors for local control, preservation of functional status, and pain relief.** *AJR Am J Roentgenol* 2017;208:453–58 CrossRef Medline
6. Frautschi R, Rampazzo A, Bernard S, et al. **Management of the salivary glands and facial nerve in face transplantation.** *Plast Reconstr Surg* 2016;137:1887–97 CrossRef Medline
7. Audolfsson T, Rodríguez-Lorenzo A, Wong C, et al. **Nerve transfers for facial transplantation: a cadaveric study for motor and sensory restoration.** *Plast Reconstr Surg* 2013;131:1231–40 CrossRef Medline
8. Rabinov JD, Barker FG, McKenna MJ, et al. **Virtual cisternoscopy: 3D MRI models of the cerebellopontine angle for lesions related to the cranial nerves.** *Skull Base* 2004;14:93–99; discussion 99 CrossRef Medline
9. Guenette JP, Seethamraju RT, Jayender J, et al. **MR imaging of the facial nerve through the temporal bone at 3T with a noncontrast ultrashort echo time sequence.** *AJNR Am J Neuroradiol* 2018; 39:1903–06 CrossRef Medline
10. McGhee RB, Chakeres DW, Schmalbrock P, et al. **The extracranial facial nerve: high resolution three-dimensional Fourier transform MR imaging.** *AJNR Am J Neuroradiol* 1993;14:465–72 Medline
11. Dailiana T, Chakeres D, Schmalbrock P, et al. **High-resolution MR of the intraparotid facial nerve and parotid duct.** *AJNR Am J Neuroradiol* 1997;18:165–72 Medline
12. Takahashi N, Okamoto K, Ohkubo M, et al. **High-resolution magnetic resonance of the extracranial facial nerve and parotid duct: demonstration of the branches of the intraparotid facial nerve and its relation to parotid tumours by MRI with a surface coil.** *Clin Radiol* 2005;60:349–54 CrossRef Medline
13. Chu J, Zhou Z, Hong G, et al. **High-resolution MRI of the intraparotid facial nerve based on a microsurface coil and a 3D reversed fast imaging with steady-state precession DWI sequence at 3T.** *AJNR Am J Neuroradiol* 2013;34:1643–48 CrossRef Medline
14. Blitz AM, Choudhri AF, Chonka ZD, et al. **Anatomic considerations, nomenclature, and advanced cross-sectional imaging techniques for visualization of the cranial nerve segments by MR imaging.** *Neuroimaging Clin N Am* 2014;24:1–15 CrossRef Medline
15. Seethamraju RT, Jagadeesan J, Kimbrell V, et al. **Motion compensated high resolution MR imaging of vagus and recurrent laryngeal nerves with novel phase-based navigation sequences.** In: *Proceedings of the Annual Meeting & Exhibition of the International Society for Magnetic Resonance in Medicine.* Singapore; May 7–13, 2016
16. Wen J, Desai NS, Jeffery D, et al. **High-resolution isotropic three-dimensional MR imaging of the extraforaminal segments of the cranial nerves.** *Magn Reson Imaging Clin N Am* 2018;26:101–19 CrossRef Medline
17. Klein A, Andersson J, Ardekani BA, et al. **Evaluation of 14 nonlinear deformation algorithms applied to human brain MRI registration.** *Neuroimage* 2009;46:786–802 CrossRef Medline
18. Besse PC, Guillouet B, Loubes J-M, et al. **Review and perspective for distance-based clustering of vehicle trajectories.** *IEEE Trans Intell Transport Syst* 2016;17:3306–17 CrossRef
19. Guenette JP. **Facial Nerve Imaging Pilot Study Data.** *Harv Dataverse* CrossRef Accessed September 29, 2019
20. Qin Y, Zhang J, Li P, et al. **3D double-echo steady-state with water excitation MR imaging of the intraparotid facial nerve at 1.5T: a pilot study.** *AJNR Am J Neuroradiol* 2011;32:1167–72 CrossRef Medline
21. Fujii H, Fujita A, Kanazawa H, et al. **Localization of parotid gland tumors in relation to the intraparotid facial nerve on 3D double-echo steady-state with water excitation sequence.** *AJNR Am J Neuroradiol* 2019;40:1037–42 CrossRef Medline
22. Bendella H, Spacca B, Rink S, et al. **Anastomotic patterns of the facial parotid plexus (PP): a human cadaver study.** *Ann Anat* 2017; 213:52–61 CrossRef Medline
23. Kalinowski M, Heverhagen JT, Rehberg E, et al. **Comparative study of MR sialography and digital subtraction sialography for benign salivary gland disorders.** *AJNR Am J Neuroradiol* 2002;23:1485–92 Medline